Compatibility of Trapped Ions and Dielectrics at Cryogenic Temperatures

M. Bruff,[1,2,*] L. Sonderhouse,[1,*] K. N. David,[1,2] J. Stuart,[1,†] D. H. Slichter,[1] and D. Leibfried[1,‡]
[1]*National Institute of Standards and Technology, 325 Broadway, Boulder, Colorado 80305, USA*
[2]*Department of Physics, University of Colorado, Boulder, Colorado 80309, USA*

(Received 17 July 2025; accepted 29 January 2026; published 6 March 2026)

We study the impact of an unshielded dielectric—here, a bare optical fiber—on a $^{40}Ca^+$ ion held several hundred microns away in a cryogenic surface electrode trap. We observe distance-dependent stray electric fields of up to a few kV/m due to the dielectric, which drift on average less than 10% per month and can be fully compensated with reasonable voltages on the trap electrodes. We observe ion motional heating rates attributable to the dielectric of ≈30 quanta per second at an ion-fiber distance of 215(4) μm and ≈1.5 MHz motional frequency. These results demonstrate the viability of using unshielded, trap-integrated dielectric objects such as miniature optical cavities or other optical elements in cryogenic surface electrode ion traps.

DOI: 10.1103/wj8m-1nlq

Trapped ions are a leading platform for scalable quantum computation [1–3] and realize some of the most accurate optical atomic clocks [4–6]. Because they can be entangled with optical photons serving as "flying qubits," trapped ions are also promising candidates for the "stationary qubit" nodes of a quantum network [7–9]. Their long coherence times [10] and high-fidelity quantum logic operations [3,11,12] are advantageous for entanglement distillation and entanglement swapping protocols [9,13], and they can be directly used in distributed quantum computing systems [14] and networks of entangled atomic clocks [15].

Bell states of remotely entangled trapped ions have been created with fidelities up to 97%, and fidelities above 99.9% appear feasible [16]. However, photon collection efficiencies have limited entanglement rates to 250 s^{-1} between systems separated by a few meters [17], far below the 10–100 kHz rate at which local quantum gates are typically performed [1–3]. Reference [17] used a high-numerical-aperture (NA) lens to collect photons emitted from the ion, with a net collection efficiency up to 10% after coupling the light into a single-mode fiber [18]. High-finesse optical cavities with a small ($\lesssim$10 μm) mode waist are an attractive alternative that can provide near-unity collection efficiency [19]. However, realizing the requisite high finesse becomes increasingly difficult for longer cavities. Shorter cavities with smaller micromachined mirrors, potentially on the ends of optical fibers, thus could be advantageous [20–29].

Trapping an ion in a shorter cavity brings it into closer proximity with the dielectric cavity mirrors and substrates, which as insulators can host static and oscillating charges on their surfaces and in the bulk. This can present a challenge, as ions are highly sensitive to the resulting electric fields [30–33]. The question of system compatibility with nearby dielectrics is relevant not only to trapped ions, including trap-integrated optical cavities [22,34–38] and trap-integrated laser delivery and fluorescence collection optics [39–51], but also to any electric-field sensitive system such as neutral Rydberg atoms [52,53] or Casimir force measurements [54]. Conductive coatings such as indium tin oxide can reduce charging but also introduce optical loss that prevents their use in high-finesse optical cavities [55,56]. Previous room-temperature experiments have measured large stray electric fields near unshielded dielectrics that drift over hours and displace the ion by hundreds of microns [57]. These stray fields are caused by charges that accumulate on the surface of the dielectric. Thermally activated fluctuators inside the dielectric bulk radiate oscillating electric fields that cause ion motional heating; the heating rate of 7×10^4 quanta/s at a 1.6 MHz mode frequency for a 250 μm ion-dielectric separation measured in Ref. [58] is high enough to impede ground state cooling, reduce coupling to the optical cavity [19,59], and impact the fidelity of ion-ion remote entanglement [16,60,61] and local two-qubit gates [62–64]. While these studies were carried out at room temperature, cryogenically operated ion traps are becoming increasingly common due to a variety of advantages [1,33,65–68] and may exhibit different behavior for trap-integrated dielectrics.

Here, we report measurements of trapped ion behavior in the presence of a nearby unshielded dielectric at cryogenic temperatures. We use a linear surface-electrode ion trap operated at ≈6.5 K with a bare optical fiber placed on top of the trap chip and aligned along the trap axis. We determine the three-dimensional stray electric field $\vec{E}$ at various ion-fiber distances d, compensate it using voltages

[*]These authors contributed equally to this work.
[†]Present address: IonQ, 4505 Campus Drive, College Park, Maryland 20740, USA.
[‡]Contact author: dietrich.leibfried@nist.gov

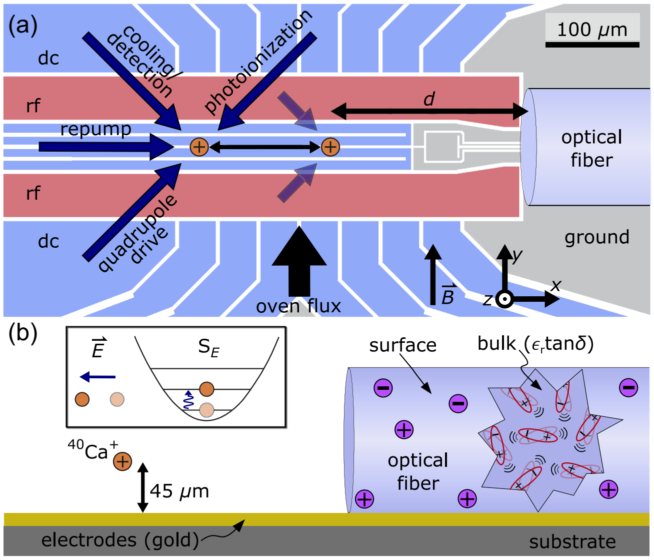

FIG. 1. Schematic of apparatus and relevant mechanisms. (a) Top view of the surface-electrode ion trap with attached bare optical fiber. An ion (orange circle) is loaded ≈325 μm from the optical fiber and transported to various ion-fiber distances d to quantify stray fields and heating rates. Directions of laser beams, neutral Ca flux, and applied magnetic field $\vec{B}$ are indicated with arrows, and laser beam orientations at the transported ion position are indicated with shorter arrows. (b) Stray charges on the optical fiber surface produce a static electric field $\vec{E}$, while thermal fluctuators inside the bulk (cutaway view) radiate electric field noise with power spectral density $S_E(\omega)$ that heats ion motion.

applied to the trap electrodes, and track an overall slow decrease over several months in the electric field magnitude along the trap axis. We fit the data with a simple model of fields from charges accumulated on the fiber surface, yielding equivalent stray charge densities similar to those reported in Ref. [57]. We also measure motional heating rates both along and perpendicular to the ion-fiber axis in a plane parallel to the electrodes for different d. The equivalent electric field noise power spectral density $S_E(\omega)$ is $\sim 10^3$ times lower than that reported in Ref. [58] for equivalent distances and mode orientations, due to a combination of the cryogenic temperature and electric field shielding from the trap electrodes themselves. Modeling the fiber as a body with uniform relative permittivity ϵ_r and dielectric loss tangent $\tan\delta$, we extract the product $\epsilon_r \tan\delta = 0.0050(7)$.

We perform these experiments using a single $^{40}\mathrm{Ca}^+$ ion loaded into a linear surface electrode trap with a bare 125-μm-diameter optical fiber (780HP) attached to the surface, in line with the trap axis as shown in Fig. 1(a) [69]. The trap and optical fiber are housed inside an ultrahigh vacuum chamber and are cooled to ≈6.5 K using a closed-cycle gaseous helium flow cryostat. The rf electrodes (red) provide confinement radially (in the y-z plane) along the rf null line, which is along the x axis ≈45 μm above the trap surface. Voltages applied to the segmented dc electrodes (blue) confine the ion axially (along x) and tilt the radial modes ≈10° from the z and y axes to enable efficient Doppler cooling of all modes. We refer to these as the "out-of-plane" and "in-plane" radial modes, respectively. Typical motional frequencies are 4–5 MHz in the radial directions and ≈1.5 MHz in the axial direction. A magnetic field of $\vec{B} \approx 0.4$ mT along y defines the quantization axis.

To study the ion behavior near the optical fiber, a $^{40}\mathrm{Ca}^+$ ion is first loaded at $d \approx 325$ μm by photoionizing neutral calcium emitted from a thermal oven using 375 nm and 423 nm laser light [79]. Loading far from the fiber reduces stray charge accumulation on the fiber surface. Voltages on the dc electrodes are then ramped to transport the ion along the rf null line, as close as $d = 215(4)$ μm. Doppler cooling and fluorescence detection are performed using 397 nm laser light to drive the $4^2S_{1/2} \leftrightarrow 4^2P_{1/2}$ transition along with 866 nm laser light to repump the population out of the metastable $3^2D_{3/2}$ state [59]. Ion fluorescence is collected with an objective (NA = 0.2) and detected with either an electron-multiplied charge-coupled device camera or a photomultiplier tube. State preparation, sideband cooling, and coherent operations are performed using the quadrupole $4^2S_{1/2} \leftrightarrow 3^2D_{5/2}$ transition, which is driven using a narrow 729 nm laser locked to an ultrastable cavity. We prepare the state $4^2S_{1/2}|m_J = -1/2\rangle \equiv |{\downarrow}\rangle$ by optical pumping with the 729 nm laser tuned to the $4^2S_{1/2}|m_J = 1/2\rangle \leftrightarrow 3^2D_{5/2}|m_J = -3/2\rangle$ transition frequency and an 854 nm repump laser. Coherent operations are then driven between $|{\downarrow}\rangle \leftrightarrow 3^2D_{5/2}|m_J = -5/2\rangle \equiv |{\uparrow}\rangle$. To quantify how the bare optical fiber modifies trapped-ion performance, we carry out a reference measurement in an identical trap without an optical fiber. The heating rates and stray electric fields observed are consistent with prior reports on this trap design [67,80]. Collectively, we refer to these measurements as the "fiber-free reference."

We use $\vec{E}$ and motional heating rates $\dot{\bar{n}}$ as a probe of static and dynamic properties of the dielectric. Figure 1(b) depicts the mechanisms we consider in our model schematically. Stray charges can accumulate on the fiber surface in several ways. Electrons can be photoelectrically dissociated from the fiber surface by stray laser light at 375 nm, 397 nm, or 423 nm, leaving a net positive surface charge. Additionally, electrons dissociated from the trap electrodes or produced from calcium atoms during photoionization, along with calcium ions that we fail to trap or other charged particles, could adsorb to the fiber surface. These charges are largely immobile on the insulating dielectric, particularly at cryogenic temperatures, and will contribute to $\vec{E}$ at the ion position. A single elementary charge on the end of the optical fiber can produce $|\vec{E}|$ as large as ≈10 mV/m at the ion position for $d = 250$ μm.

Inside the bulk of the fiber, an ensemble of thermally excited fluctuators with electric dipole moments radiate a time-dependent electric field that can excite the motion of

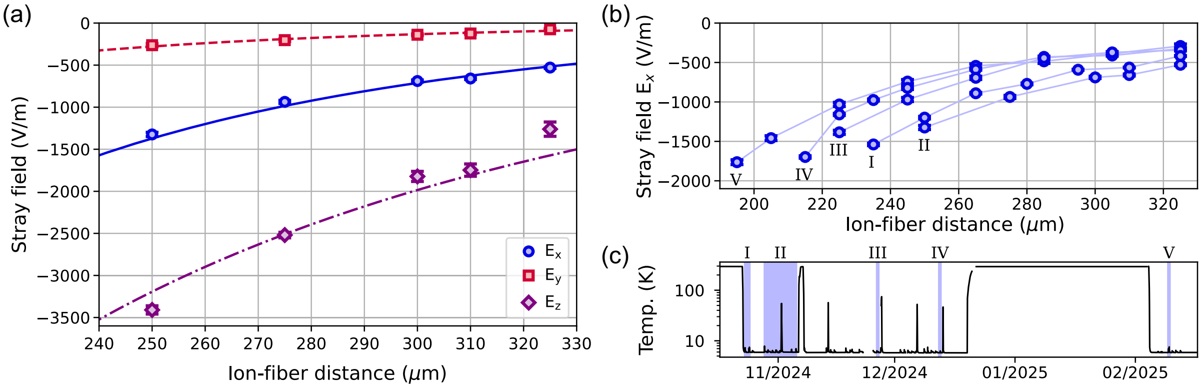

FIG. 2. Distance dependence of the stray electric field $\vec{E}$. (a) Stray field data in the x (blue circles), y (red squares), and z (purple diamonds) directions. The fitted E_x, E_y, and E_z are shown as lines in solid blue, dashed red, and dot-dashed purple, respectively. (b) E_x from five sequential data runs [labeled I–V, where II is the data run in (a)], with connecting lines to guide the eye, showing a slow relaxation over several months. Some error bars are smaller than the plot markers. (c) Temperature T of the trap and optical fiber over the time period of the data runs shown in (b), including both full and partial cycles between ≈6 and 300 K. All error bars represent 68% confidence intervals.

the trapped ion. These electric field fluctuations can be described by their power spectral density at the ion position $S_E(\omega, \hat{\beta})$ (in $V^2\ m^{-2}\ Hz^{-1}$) at angular frequency ω along the unit vector $\hat{\beta}$. Since direct calculation of $S_E(\omega, \hat{\beta})$ can be difficult, we use the fluctuation dissipation theorem to determine $S_E(\omega, \hat{\beta})$ by instead calculating the change in the electric field from the ion $\vec{E}_{\mathrm{ion}}(\vec{r}, \vec{r}')$ seen at position $\vec{r}'$ inside the dielectric bulk due to the ion being displaced along $\hat{\beta}$ from its equilibrium position $\vec{r}$ [58,81]:

$$S_E(\omega, \hat{\beta}) = \frac{4k_B T}{q^2 \omega} \epsilon_0 \epsilon_r \tan\delta \int_V \sum_i \left| \sum_j \frac{\partial E_{\mathrm{ion},i}}{\partial r_j} \beta_j \right|^2 d^3\vec{r}'. \qquad (1)$$

The integral is taken over the volume V of the dielectric bulk, and i and j index over the three spatial dimensions. Here, k_B is the Boltzmann constant, T is the temperature of the dielectric, q is the ion charge, ϵ_0 is the vacuum permittivity, and $\epsilon_r \tan\delta$ is the imaginary part of the complex relative permittivity of the dielectric. This power spectral density is related to the motional heating rate $\dot{\bar{n}}$ for a mode along axis $\hat{\beta}$ at angular frequency ω according to [30,33]

$$\dot{\bar{n}} = \frac{q^2}{4m\hbar\omega} S_E(\omega, \hat{\beta}), \qquad (2)$$

where m is the ion mass and $\hbar$ is the reduced Planck's constant. Equations (1) and (2) connect the measured heating rates to the intrinsic dielectric properties given the trap and dielectric geometry.

In Fig. 2(a), the three components of $\vec{E}$ are determined at various ion-fiber distances by adding compensation voltages to the applied voltages on the dc electrodes so that the ion's equilibrium position is at the rf null in the y-z plane and the unperturbed dc well minimum in x [69]. Data for a single ion-fiber distance were taken on the same day, while the full set of measurements was completed within one week. The stray fields are small enough that we can compensate them fully in all three directions over the full range of ion-fiber distances shown without exceeding ±10 V applied to the dc electrodes. The position of the optical fiber on the trap influences the magnitude of $\vec{E}$. E_y is small relative to the other components due to the approximate y symmetry of the optical fiber about the rf null line, while E_z is the largest component because the field lines from the fiber terminate in the z direction at the trap surface, normal to the conducting trap electrodes.

We can make a simple model for the origin of $\vec{E}$ by assuming a stray charge distribution on the fiber with uniform values of surface charge on the end facet, the sidewall with $y > 0$, and the sidewall with $y < 0$, where $y = 0$ is along the rf null line [69]. We use electrostatic finite element simulations to calculate the resulting field strengths. We also assume an additional unknown uniform "offset" field $\vec{E}_0$ in three dimensions to account for the nonzero stray field typically seen in surface electrode traps. Fitting to the experimental data yields charge densities $\sigma_f = 9.5(6)e/\mu m^2$, $\sigma_{+\hat{y}} = 47(9)e/\mu m^2$, and $\sigma_{-\hat{y}} = -28(9)e/\mu m^2$ for the three regions, respectively, where e is the elementary charge, while the offset field from the trap is $\vec{E}_0 = (190 \pm 60, 20 \pm 50, 620 \pm 210)$ V/m. The offset field is consistent with the measured stray fields from the fiber-free reference. Despite reduced charge mobility at lower temperatures, the stray charge densities on the optical fiber are of the same order of magnitude as those imputed from room-temperature ion trap experiments in Ref. [57]. This may be due to reduced charging mechanisms in our setup, such as loading ions far from the optical fiber, or due to the presence of other nearby cold surfaces to which stray charge can adhere.

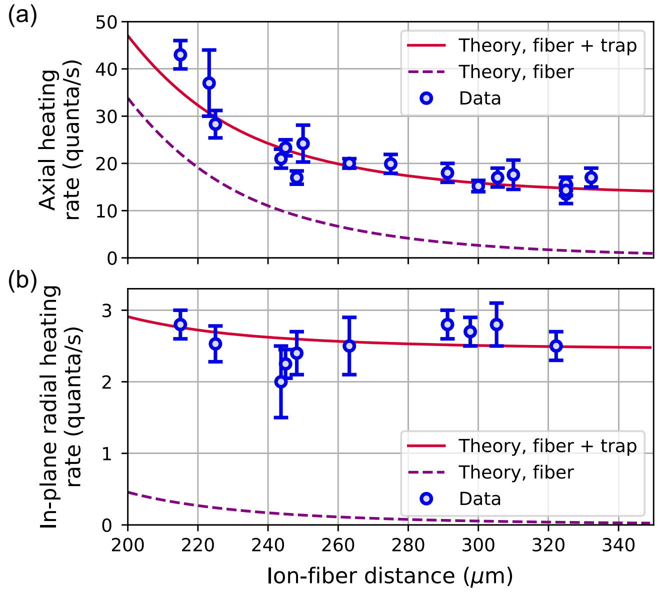

FIG. 3. Heating rates versus ion-fiber distance in the (a) axial and (b) in-plane radial directions. The axial data are fit with a model based on thermal fluctuations inside the optical fiber bulk plus a constant heating rate from the trap (red line). The radial data are fitted only to determine the constant heating rate from the trap, with the fiber contribution calculated using the dielectric properties from the axial fit. The axial [radial] data are taken with $\omega/2\pi = 1.45(5)$ MHz [4.5(6) MHz], where the error bars represent 68% confidence intervals. The fitted heating rate from the optical fiber alone is shown in both panels (purple dashed line).

We repeat the E_x measurements over multiple months, as shown in Fig. 2(b), and observe a slow relaxation with average drift rate $< 10\%$ per month, even over multiple loading attempts and temperature cycles as shown in Fig. 2(c). The long-term drift of E_y and E_z is similar to that of E_x [69]. We observe nonmonotonic drift around data run II [Fig. 2(a)], which used a higher duty cycle of 397 nm laser exposure and a higher frequency of ion loading attempts, both of which may have strengthened the stray field. The increased stability of the stray fields compared to those reported in Ref. [57] could be due to reduced charge mobility at cryogenic temperatures.

We turn now to probing the time-dependent electric field noise from the fiber with the ion's motion. Previous room-temperature experiments that trapped ions near an optical fiber found that motional heating from the dielectric was too large to allow ground state cooling [56,58]. We are able to sideband cool the axial and in-plane radial modes to $\bar{n} < 0.1$ for all ion-fiber distances shown in Fig. 3. Ground state cooling of the out-of-plane radial mode was limited to $\bar{n} < 0.5$ by the small projection of the quadrupole drive laser beam. The motional heating rates were determined using sideband thermometry [30,82,83] and were taken after radial field compensation and at consistent mode frequencies of $\omega/2\pi = 1.45(5)$ (axial) and 4.5(6) (in-plane radial) MHz. We measure axial heating rates <50 quanta/s at $d = 215(4)$ μm. We observe higher heating rates when the radial stray fields are not well compensated, likely due to technical noise on the trap rf drive. The minimum d in Fig. 3 is constrained by the compensation limit of ≈ 4 kV/m given the dc-voltage limits of ± 10 V.

The heating rate due to the dielectric is modeled via the fluctuation-dissipation mechanism, as described in Eqs. (1) and (2). Following the approach in Ref. [58], we compute the integral numerically using finite-element analysis software, using the exact surface trap geometry and optical fiber position with all electrodes grounded. Operating at 6.5 K results in a roughly 50-fold reduction in $S_E(\omega)$ relative to room temperature. Most field lines that emanate from the dielectric terminate on the conducting trap surface due to the trap's geometry relative to the fiber and ion, reducing S_E by an additional factor of $\approx 4\,(10)$ at $d = 200$ μm (350 μm) when we include the trap electrodes in our simulations [69].

Since, to the best of our knowledge, there are no data on the cryogenic dielectric properties of optical fiber at megahertz frequencies in the literature, we fit the axial heating rate data with $\epsilon_r \tan\delta$ as a free parameter. We also include a constant offset $\dot{\bar{n}}_{0,a}$ to account for the heating rate from the surface trap. From this fit, we extract $\epsilon_r \tan\delta = 0.0050(7)$. Assuming $\epsilon_r = 3.9$, the room-temperature value [84], we determine a loss tangent of $\tan\delta = 1.3(2) \times 10^{-3}$. Both the measured heating rate at $d = 330$ μm and the fitted value $\dot{\bar{n}}_{0,a} = 13(1)$ quanta/s are consistent with the measured heating rates from the fiber-free reference, indicating negligible contributions from the optical fiber.

Because of the symmetry of the optical fiber with respect to the ion, thermal fluctuations in the optical fiber contribute minimally to the heating rate of the in-plane radial mode. As a result, we model the radial heating rate data by adding the dielectric heating, calculated without free parameters using the dielectric properties from the axial heating rate fit, to a constant trap background $\dot{\bar{n}}_{0,r}$ that is the sole free parameter in the fit. We fit $\dot{\bar{n}}_{0,r} = 2.5(1)$ quanta/s. Although other heating mechanisms, such as technical noise or surface effects on the optical fiber, may contribute, our data are largely consistent with the fluctuation-dissipation model.

We also study the frequency dependence of the axial heating rate at two fixed positions: one near the fiber with $d = 225(4)$ μm and another far from the fiber at $d = 325(4)$ μm. Far from the fiber, we fit the frequency scaling to a power law, $\dot{\bar{n}}_{\rm far} = B_{\rm far}\omega^{\alpha_{\rm far}}$ with $\alpha_{\rm far} = -2.5(2)$. In light of the asymptotic behavior of the axial heating rate at larger d [Fig. 3(a)], we assume the frequency scaling far from the fiber is that of the trap. This frequency scaling is consistent with the typical frequency dependence of heating rates observed in surface-electrode ion traps [33].

Near the fiber, we treat the heating rate as a sum of effects from the trap and fiber, each with independent

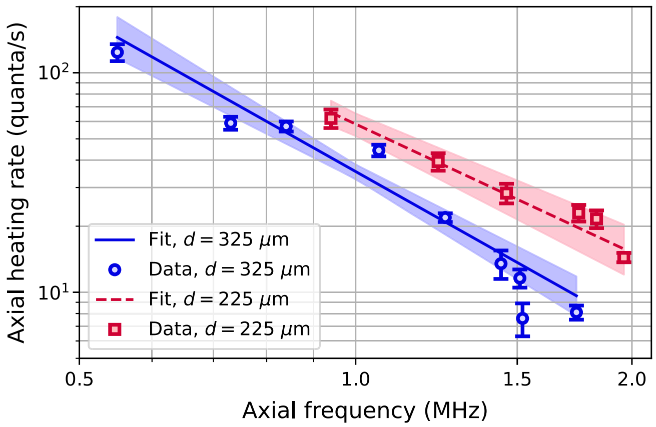

FIG. 4. Frequency dependence of axial heating rate at an ion position far from the fiber [$d = 325(4)$ μm, blue circles] and near the fiber [$d = 225(4)$ μm, red squares] with corresponding power law fits to the data (blue solid and red dashed lines) and 68% confidence intervals (shaded regions).

power law frequency dependence:

$$\dot{\bar{n}}_{\mathrm{near}}(\omega) = B_{\mathrm{trap}}\omega^{\alpha_{\mathrm{trap}}} + B_{\mathrm{fib}}\omega^{\alpha_{\mathrm{fib}}}. \tag{3}$$

We can choose to use the values extracted far from the fiber for the trap parameters, $B_{\mathrm{trap}} = B_{\mathrm{far}}$ and $\alpha_{\mathrm{trap}} = \alpha_{\mathrm{far}}$, yielding $\alpha_{\mathrm{fib}} = -1.5(5)$. However, since the magnitude and frequency dependence of the trap heating rate may be ion-position dependent, we can alternatively fit the frequency dependence of heating rates near the fiber to a single power law, $\dot{\bar{n}}_{\mathrm{near}} = B_{\mathrm{near}}\omega^{\alpha_{\mathrm{near}}}$. This gives $\alpha_{\mathrm{near}} = -1.9(2)$ and is the fit included in Fig. 4. In both analyses, the heating rate frequency scaling is consistent with the prediction from the fluctuation dissipation theorem of $\alpha = -2$ to within the fit uncertainty.

Our results show the feasibility of trapping ions near large dielectric objects with manageable ion heating rates and stray electric fields, opening the door for devices such as trap-integrated high-finesse optical cavities with ion-mirror distances of several hundred microns. Simulations predict that the increase in motional heating due to the dielectric mirror coating in such a cavity should be small [69]. With the potential for high single-ion cooperativity and low motional heating rates, such trap-integrated cavities would be suitable for high-fidelity, high-rate quantum networking applications and cavity quantum electrodynamics studies with trapped ions.

Acknowledgments—The authors thank Andrew Wilson for important early contributions to the project, Giorgio Zarantonello for design and assembly of the experimental apparatus, and Chin-Wen Chou and Zhimin Liu for maintaining the ultrastable cavity. M. B. is an associate in the Professional Research Experience Program (PREP) operated jointly by NIST and the University of Colorado. L. S. acknowledges support from a National Research Council postdoctoral fellowship. K. N. D. acknowledges support from the NSF Quantum Leap Challenge Institute Award No. OMA-2016244. This work was supported by the NIST Quantum Network Grand Challenge.

M. B. and L. S. performed the experiments, analyzed the data, and wrote the manuscript. L. S., with assistance from K. N. D., completed the simulations. D. H. S. designed and fabricated the trap. K. N. D. and D. H. S. assembled the fiber on the trap. J. S. and L. S. designed and built the apparatus. All authors contributed to experimental design and manuscript editing. D. H. S. and D. L. secured funding for the work. D. L., D. H. S., and L. S. supervised the work.

Data availability—The data that support the findings of this article are not publicly available upon publication because it is not technically feasible and/or the cost of preparing, depositing, and hosting the data would be prohibitive within the terms of this research project. The data are available from the authors upon reasonable request.

[1] S. A. Moses, C. H. Baldwin *et al.*, Phys. Rev. X **13**, 041052 (2023).
[2] J.-S. Chen, E. Nielsen, M. Ebert, V. Inlek, K. Wright, V. Chaplin, A. Maksymov, E. Paez, A. Poudel, P. Maunz, and J. Gamble, Quantum **8**, 1516 (2024).
[3] C. M. Löschnauer, J. Mosca Toba, A. C. Hughes, S. A. King, M. A. Weber, R. Srinivas, R. Matt, R. Nourshargh, D. T. C. Allcock, C. J. Ballance, C. Matthiesen, M. Malinowski, and T. P. Harty, PRX Quantum **6**, 040313 (2025).
[4] M. C. Marshall, D. A. R. Castillo, W. J. Arthur-Dworschack, A. Aeppli, K. Kim, D. Lee, W. Warfield, J. Hinrichs, N. V. Nardelli, T. M. Fortier *et al.*, Phys. Rev. Lett. **135**, 033201 (2025).
[5] N. Huntemann, C. Sanner, B. Lipphardt, C. Tamm, and E. Peik, Phys. Rev. Lett. **116**, 063001 (2016).
[6] H. N. Hausser, J. Keller, T. Nordmann, N. M. Bhatt, J. Kiethe, H. Liu, I. M. Richter, M. von Boehn, J. Rahm, S. Weyers *et al.*, Phys. Rev. Lett. **134**, 023201 (2025).
[7] L.-M. Duan, M. Lukin, J. Cirac, and P. Zoller, Nature (London) **414**, 413 (2001).
[8] L.-M. Duan, B. B. Blinov, D. L. Moehring, and C. R. Monroe, Quantum Inf. Comput. **4**, 165 (2004).
[9] H. J. Briegel, W. Dür, J. I. Cirac, and P. Zoller, Phys. Rev. Lett. **81**, 5932 (1998).
[10] P. Wang, C.-Y. Luan, M. Qiao, M. Um, J. Zhang, Y. Wang, X. Yuan, M. Gu, J. Zhang, and K. Kim, Nat. Commun. **12**, 233 (2021).
[11] M. C. Smith, A. D. Leu, K. Miyanishi, M. F. Gely, and D. M. Lucas, Phys. Rev. Lett. **134**, 230601 (2025).
[12] C. R. Clark, H. N. Tinkey, B. C. Sawyer, A. M. Meier, K. A. Burkhardt, C. M. Seck, C. M. Shappert, N. D. Guise, C. E. Volin, S. D. Fallek *et al.*, Phys. Rev. Lett. **127**, 130505 (2021).

[13] C. H. Bennett, G. Brassard, S. Popescu, B. Schumacher, J. A. Smolin, and W. K. Wootters, Phys. Rev. Lett. **76**, 722 (1996).

[14] C. Monroe, R. Raussendorf, A. Ruthven, K. R. Brown, P. Maunz, L. M. Duan, and J. Kim, Phys. Rev. A **89**, 022317 (2014).

[15] B. C. Nichol, R. Srinivas, D. P. Nadlinger, P. Drmota, D. Main, G. Araneda, C. J. Ballance, and D. M. Lucas, Nature (London) **609**, 689 (2022).

[16] S. Saha, M. Shalaev, J. O'Reilly, I. Goetting, G. Toh, A. Kalakuntla, Y. Yu, and C. Monroe, Nat. Commun. **16**, 2533 (2025).

[17] J. O'Reilly, G. Toh, I. Goetting, S. Saha, M. Shalaev, A. L. Carter, A. Risinger, A. Kalakuntla, T. Li, A. Verma, and C. Monroe, Phys. Rev. Lett. **133**, 090802 (2024).

[18] A. L. Carter, J. O'Reilly, G. Toh, S. Saha, M. Shalaev, I. Goetting, and C. Monroe, Rev. Sci. Instrum. **95**, 033201 (2024).

[19] J. Schupp, V. Krcmarsky, V. Krutyanskiy, M. Meraner, T. E. Northup, and B. P. Lanyon, PRX Quantum **2**, 020331 (2021).

[20] D. Hunger, T. Steinmetz, Y. Colombe, C. Deutsch, T. Hänsch, and J. Reichel, New J. Phys. **12**, 065038 (2010).

[21] M. Brekenfeld, D. Niemietz, J. D. Christesen, and G. Rempe, Nature (London) **16**, 647 (2020).

[22] P. Kobel, M. Breyer, and M. Köhl, npj Quantum Inf. **7**, 6 (2021).

[23] H. Pfeifer, L. Ratschbacher, J. Gallego, C. Saavedra, A. Faßbender, A. von Haaren, W. Alt, S. Hofferberth, M. Köhl, S. Linden, and D. Meschede, Appl. Phys. B **128**, 29 (2022).

[24] D. Riedel, I. Söllner, B. J. Shields, S. Starosielec, P. Appel, E. Neu, P. Maletinsky, and R. J. Warburton, Phys. Rev. X **7**, 031040 (2017).

[25] C. Deshmukh, E. Beattie, B. Casabone, S. Grandi, D. Serrano, A. Ferrier, P. Goldner, D. Hunger, and H. de Riedmatten, Optica **10**, 1339 (2023).

[26] S. Gao, J. A. Blackmore, W. J. Hughes, T. H. Doherty, and J. F. Goodwin, Phys. Rev. Appl. **19**, 014033 (2023).

[27] D. J. Kay, S. J. Snowden, G. Stutter, and M. K. Keller, Opt. Express **32**, 43654 (2024).

[28] B. Grinkemeyer, E. Guardado-Sanchez, I. Dimitrova, D. Shchepanovich, E. Mandopoulou, G. J. Borregaard, V. Vuletić, and M. D. Lukin, Science **387**, 1301 (2025).

[29] S. Gao, V. Kavungal, S. Oya, D. Okuno, E. Kassa, W. J. Hughes, P. Horak, and H. Takahashi, Opt. Express **33**, 39009 (2025).

[30] Q. A. Turchette, D. Kielpinski, B. E. King, D. Leibfried, D. M. Meekhof, C. J. Myatt, M. A. Rowe, C. A. Sackett, C. S. Wood, W. M. Itano, C. Monroe, and D. J. Wineland, Phys. Rev. A **61**, 063418 (2000).

[31] G. Huber, F. Ziesel, U. Poschinger, K. Singer, and F. Schmidt-Kaler, Appl. Phys. B **100**, 725 (2010).

[32] S. Narayanan, N. Daniilidis, S. A. Möller, R. Clark, F. Ziesel, K. Singer, F. Schmidt-Kaler, and H. Häffner, J. Appl. Phys. **110**, 114909 (2011).

[33] M. Brownnutt, M. Kumph, P. Rabl, and R. Blatt, Rev. Mod. Phys. **87**, 1419 (2015).

[34] J. D. Sterk, L. Luo, T. A. Manning, P. Maunz, and C. Monroe, Phys. Rev. A **85**, 062308 (2012).

[35] A. Van Rynbach, P. Maunz, and J. Kim, Appl. Phys. Lett. **109**, 221108 (2016).

[36] M. Teller, V. Messerer, K. Schüppert, Y. Zou, D. A. Fioretto, M. Galli, P. C. Holz, J. Reichel, and T. E. Northup, AVS Quantum Sci. **5**, 012001 (2023).

[37] H. Takahashi, E. Kassa, C. Christoforou, and M. Keller, Phys. Rev. Lett. **124**, 013602 (2020).

[38] E. Kassa, S. Gao, S. Teh, D. van Dinter, and H. Takahashi, Phys. Rev. Appl. **23**, 024038 (2025).

[39] G. Brady, A. R. Ellis, D. L. Moehring, D. Stick, C. Highstrete, K. M. Fortier, M. G. Blain, R. A. Haltli, A. A. Cruz-Cabrera, R. D. Briggs, J. R. Wendt, T. R. Carter, S. Samora, and S. A. Kenne, Appl. Phys. B **103**, 801 (2011).

[40] T. H. Kim, P. F. Herskind, and I. L. Chuang, Appl. Phys. Lett. **98**, 214103 (2011).

[41] A. P. VanDevender, Y. Colombe, J. Amini, D. Leibfried, and D. J. Wineland, Phys. Rev. Lett. **105**, 023001 (2010).

[42] A. Jechow, E. W. Streed, B. G. Norton, M. J. Petrasiunas, and D. Kielpinski, Opt. Lett. **36**, 1371 (2011).

[43] H. Takahashi, A. Wilson, A. Riley-Watson, F. Oručević, N. Seymour-Smith, M. Keller, and W. Lange, New J. Phys. **15**, 053011 (2013).

[44] P. Bado, Fused silica ion trap chip with efficient optical collection system for timekeeping, sensing, and emulation, Technical Report No. FA9550-12-C-0074, 2015.

[45] K. K. Mehta, C. D. Bruzewicz, R. McConnell, R. J. Ram, J. M. Sage, and J. Chiaverini, Nat. Nanotechnol. **11**, 1066 (2016).

[46] R. J. Niffenegger, J. Stuart, C. Sorace-Agaskar, D. Kharas, S. Bramhavar, C. D. Bruzewicz, W. Loh, R. T. Maxson, R. McConnell, D. Reens *et al.*, Nature (London) **586**, 538 (2020).

[47] K. K. Mehta, C. Zhang, M. Malinowski, T.-L. Nguyen, M. Stadler, and J. P. Home, Nature (London) **586**, 533 (2020).

[48] M. L. Day, K. Choonee, Z. Chaboyer, S. Gross, M. J. Withford, A. G. Sinclair, and G. D. Marshall, Quantum Sci. Technol. **6**, 024007 (2021).

[49] F. W. Knollmann, E. Clements, P. T. Callahan, M. Gehl, J. D. Hunker, T. Mahony, R. McConnell, R. Swint, C. Sorace-Agaskar, I. L. Chuang, J. Chiaverini, and D. Stick, Opt. Quantum **2**, 230 (2024).

[50] R. Bushati *et al.*, in *Emerging Applications in Silicon Photonics IV*, edited by C. G. Littlejohns and M. Sorel, International Society for Optics and Photonics (SPIE, 2023), Vol. 12794, p. 127940G.

[51] D. Fang, W.-B. Chen, C.-H. Zhang, J.-M. Cui, Y.-F. Huang, C.-F. Li, and G.-C. Guo, Phys. Rev. Appl. **24**, 024037 (2025).

[52] H. Bernien, S. Schwartz, A. Keesling, H. Levine, A. Omran, H. Pichler, S. Choi, A. S. Zibrov, M. Endres, M. Greiner, V. Vuletić, and M. D. Lukin, Nature (London) **551**, 579 (2017).

[53] F. Gu, S. G. Menon, D. Maier, A. Das, T. Chakraborty, W. Tittel, H. Bernien, and J. Borregaard, npj Quantum Inf. **11**, 182 (2025).

[54] J. L. Garrett, J. Kim, and J. N. Munday, Phys. Rev. Res. **2**, 023355 (2020).

[55] A. M. Eltony, S. X. Wang, G. M. Akselrod, P. F. Herskind, and I. L. Chuang, Appl. Phys. Lett. **102**, 054106 (2013).

[56] W.-B. Chen, D. Fang, C.-H. Zhang, J.-M. Cui, Y.-F. Huang, C.-F. Li, and G.-C. Guo, Quantum Sci. Technol. **11**, 015045 (2026).
[57] F. R. Ong, K. Schüppert, P. Jobez, M. Teller, B. Ames, D. A. Fioretto, K. Friebe, M. Lee, Y. Colombe, R. Blatt, and T. E. Northup, New J. Phys. **22**, 063018 (2020).
[58] M. Teller, D. A. Fioretto, P. C. Holz, P. Schindler, V. Messerer, K. Schüppert, Y. Zou, R. Blatt, J. Chiaverini, J. Sage, and T. E. Northup, Phys. Rev. Lett. **126**, 230505 (2021).
[59] C. Roos, Controlling the quantum state of trapped ions, Ph.D. thesis, University of Innsbruck, 2000.
[60] J. Apolín and D. P. Nadlinger, arXiv:2503.16837.
[61] S. Kikura, R. Inoue, H. Yamasaki, A. Goban, and S. Sunami, PRX Quantum **6**, 040351 (2025).
[62] A. Sørensen and K. Mølmer, Phys. Rev. Lett. **82**, 1971 (1999).
[63] A. Sørensen and K. Mølmer, Phys. Rev. A **62**, 022311 (2000).
[64] G. J. Milburn, S. Schneider, and D. F. V. James, Fortschr. Phys. **48**, 801 (2000).
[65] G. Pagano, P. W. Hess, H. B. Kaplan, W. L. Tan, P. Richerme, P. Becker, A. Kyprianidis, J. Zhang, E. Birckelbaw, M. R. Hernandez, Y. Wu, and C. Monroe, Quantum Sci. Technol. **4**, 014004 (2018).
[66] T. Dubielzig, S. Halama, H. Hahn, G. Zarantonello, M. Niemann, A. Bautista-Salvador, and C. Ospelkaus, Rev. Sci. Instrum. **92**, 043201 (2021).
[67] S. Todaro, Scalable state detection and fast transport of trapped-ion qubits for quantum computing, Ph.D. thesis, University of Colorado at Boulder, 2020.
[68] L. Deslauriers, S. Olmschenk, D. Stick, W. K. Hensinger, J. Sterk, and C. Monroe, Phys. Rev. Lett. **97**, 103007 (2006).
[69] See Supplemental Material at http://link.aps.org/supplemental/10.1103/wj8m-1nlq for specifics on the optical fiber attachment, radial stray field drift, details of the stray charge density model, and additional simulations of the dielectric-induced heating rate. Supplemental Material includes additional Refs. [70–78].
[70] H. M. Knaack, Laser-free operations in a mixed-species trapped ion processor, Ph.D. thesis, University of Colorado Boulder, 2024.
[71] J. Chiaverini, R. B. Blakestad, J. Britton, J. D. Jost, C. Langer, D. Leibfried, R. Ozeri, and D. J. Wineland, Quantum Inf. Comput. **5**, 419 (2005).
[72] J. H. Wesenberg, Phys. Rev. A **78**, 063410 (2008).
[73] M. G. House, Phys. Rev. A **78**, 033402 (2008).
[74] J. P. Home, D. Hanneke, J. D. Jost, D. Leibfried, and D. J. Wineland, New J. Phys. **13**, 073026 (2011).
[75] D. J. Berkeland, J. D. Miller, J. C. Bergquist, W. M. Itano, and D. J. Wineland, J. Appl. Phys. **83**, 5025 (1998).
[76] G. Rempe, R. J. Thompson, H. J. Kimble, and R. Lalezari, Opt. Lett. **17**, 363 (1992).
[77] J.-Y. Kim, A. Garg, E. Rymaszewski, and T.-M. Lu, IEEE Trans. Compon. Packag. Technol. **24**, 526 (2001).
[78] P. Jain and E. J. Rymaszewski, Applications, in *Thin-Film Capacitors for Packaged Electronics* (Springer US, Boston, 2004), pp. 145–153.
[79] S. Gulde, D. Rotter, P. Barton, F. Schmidt-Kaler, R. Blatt, and W. Hogervorst, Appl. Phys. B **73**, 861 (2001).
[80] S. L. Todaro, V. B. Verma, K. C. McCormick, D. T. C. Allcock, R. P. Mirin, D. J. Wineland, S. W. Nam, A. C. Wilson, D. Leibfried, and D. H. Slichter, Phys. Rev. Lett. **126**, 010501 (2021).
[81] M. Kumph, C. Henkel, P. Rabl, M. Brownnutt, and R. Blatt, New J. Phys. **18**, 023020 (2016).
[82] C. Monroe, D. M. Meekhof, B. E. King, S. R. Jefferts, W. M. Itano, D. J. Wineland, and P. Gould, Phys. Rev. Lett. **75**, 4011 (1995).
[83] D. Leibfried, R. Blatt, C. Monroe, and D. Wineland, Rev. Mod. Phys. **75**, 281 (2003).
[84] P. Jain and E. J. Rymaszewski, Electrical characterization, in *Thin-Film Capacitors for Packaged Electronics* (Springer US, Boston, MA, 2004), pp. 91–119.